Strong and highly variable push of ocean waves on Southern Ocean sea ice

Justin E. Stopa[a,1,2], **Peter Sutherland**[a], **and Fabrice Ardhuin**[a]

[a]Laboratoire d'Océanographie Physique et Spatiale (LOPS), l'Université de Bretagne Occidentale (UBO), CNRS, IRD, l'Institut Français de Recherche pour l'Exploitation de la Mer (IFREMER), 29280 Plouzane, France

Edited by Claire L. Parkinson, NASA/Goddard Space Flight Center, Greenbelt, MD, and approved April 16, 2018 (received for review February 2, 2018)

Sea ice in the Southern Ocean has expanded over most of the past 20 y, but the decline in sea ice since 2016 has taken experts by surprise. This recent evolution highlights the poor performance of numerical models for predicting extent and thickness, which is due to our poor understanding of ice dynamics. Ocean waves are known to play an important role in ice break-up and formation. In addition, as ocean waves decay, they cause a stress that pushes the ice in the direction of wave propagation. This wave stress could not previously be quantified due to insufficient observations at large scales. Sentinel-1 synthetic aperture radars (SARs) provide high-resolution imagery from which wave height is measured year round encompassing Antarctica since 2014. Our estimates give an average wave stress that is comparable to the average wind stress acting over 50 km of sea ice. We further reveal highly variable half-decay distances ranging from 400 m to 700 km, and wave stresses from 0.01 to 1 Pa. We expect that this variability is related to ice properties and possibly different floe sizes and ice thicknesses. A strong feedback of waves on sea ice, via break-up and rafting, may be the cause of highly variable sea-ice properties.

wave–ice interaction | Southern Ocean marginal ice zone | wave radiation stress | Sentinel-1 SAR | synthetic aperture radar

Antarctic sea ice is changing. Its extent increased from the beginning of the satellite record until 2014 (1–3), followed by a dramatic retreat (4). This variability is poorly captured by current climate models (5, 6). Also, these models fail to explain the presence of thick ice (7). These shortcomings point to missing or improperly resolved physical processes.

Dynamic processes acting on sea ice involve wind (8), ocean circulation (9), and ocean waves (10). Here we focus on the role of waves on the ice, within a few hundreds of kilometers of the ice edge. Waves are generated by winds over ice-free oceans and can propagate long distances (11), including into ice-covered waters (10). This propagation redistributes the momentum gained from the wind over large regions. Waves attenuated by sea ice, or by any floating body (12), impart to the ice their excess of momentum. Theoretical calculations and numerical modeling show that this stress impacts the ice edge (13–15). The observation of wave heights in the ice can provide a direct estimate of the wave-induced stress, but it has so far been limited to a few in situ experiments (10, 16, 17).

The European Space Agency's Sentinel-1 (S1) constellation consists of two satellites carrying Synthetic Aperture Radars (SARs). They operate over most of the oceans in a 4-m resolution "wave mode" that is designed to monitor ocean waves (11). The wave mode provides 20×20 km images every 100 km along the satellite orbit, revealing stunning details of air–sea interaction processes. Soon after launch in 2014, the S1A acquisition cycle was modified to extend wave mode coverage over Antarctic Sea ice. S1A was followed by S1B in 2016.

Satellite-based SAR imagery has been used to study wave–ice interaction starting with Seasat in 1978 (18) and with European remote sensing satellite 2 (ERS2) (19). The new higher resolution Sentinel images motivated further analysis of wave in ice patterns, leading to a quantitative estimation method for the directional wave spectrum, from which wave heights, periods, and directions can be derived (20–23). This method, applied to S1A and S1B wave mode data, provides a year-round dataset of wave heights and wave stresses that covers all of the Antarctic sea ice (see *Methods* and *SI Appendix* for details). This dataset is unique because it contains a wide range of sea states and ice conditions for all months around the entire Southern Ocean.

Fig. 1 shows two representative SAR images, one with an abrupt decrease in wave amplitude (Fig. 1*A*) and the other with a nearly constant wave field across the image (Fig. 1*D*). Both images are in ice-covered seas located at least 130 km from the ice edge. Vertical motions of the ice produce a Doppler shift in the radar echo, in addition to the Doppler shift induced by the satellite motion. SAR processing gives high resolution in azimuth by placing echoes according to their Doppler shift; hence, moving targets are displaced along the azimuth direction, in proportion to their velocities. This explains the wave-like patterns in the radar image: they are due to the wave orbital velocities' effect on radar processing and would not be visible in optical imagery. We analyzed 52,845 wave mode SAR scenes in sea ice, of which 12,650 (24%) contain wave features. Images with multiple wave trains, dominant ice morphological features, and unresolved short waves are not included in the analysis, leaving 2,237 (5%) images that contain single swell systems, well imaged by the SARs (see *SI Appendix*), for which we estimate a surface elevation variance E at a resolution of 2 km. To study wave attenuation (and stress), the incoming sea state must be estimated. The incoming wave variance E_0 is derived from the nearest open ocean SAR image using a proven method used for

Significance

Southern Ocean sea ice plays a key role in regulating the uptake of carbon and heat by the global ocean. In this context, ocean waves have a strong influence, including ice break-up and pancake formation. These processes explain large differences in sea-ice properties between Arctic and Antarctic. Waves also decay in the ice, exerting a force in their propagation direction that compacts the ice. Here, we provide an extensive dataset on wave heights and its decay in sea ice, using satellite imagery. Wave decay can be much faster than previously reported but is highly variable. The resulting wave force on the ice can have a profound impact on both ice extent and thickness.

Author contributions: J.E.S., P.S., and F.A. designed research; J.E.S. performed research; J.E.S. and F.A. contributed new analytic tools; J.E.S. analyzed data; and J.E.S., P.S., and F.A. wrote the paper.

The authors declare no conflict of interest.

This article is a PNAS Direct Submission.

[1]To whom correspondence should be addressed. Email: stopa@hawaii.edu.

[2]Present address: Department of Ocean Resources and Engineering, School of Ocean and Earth Science and Technology, University of Hawaii at Manoa, Honolulu, HI 96822.

This article contains supporting information online at www.pnas.org/lookup/suppl/doi:10.1073/pnas.1802011115/-/DCSupplemental.

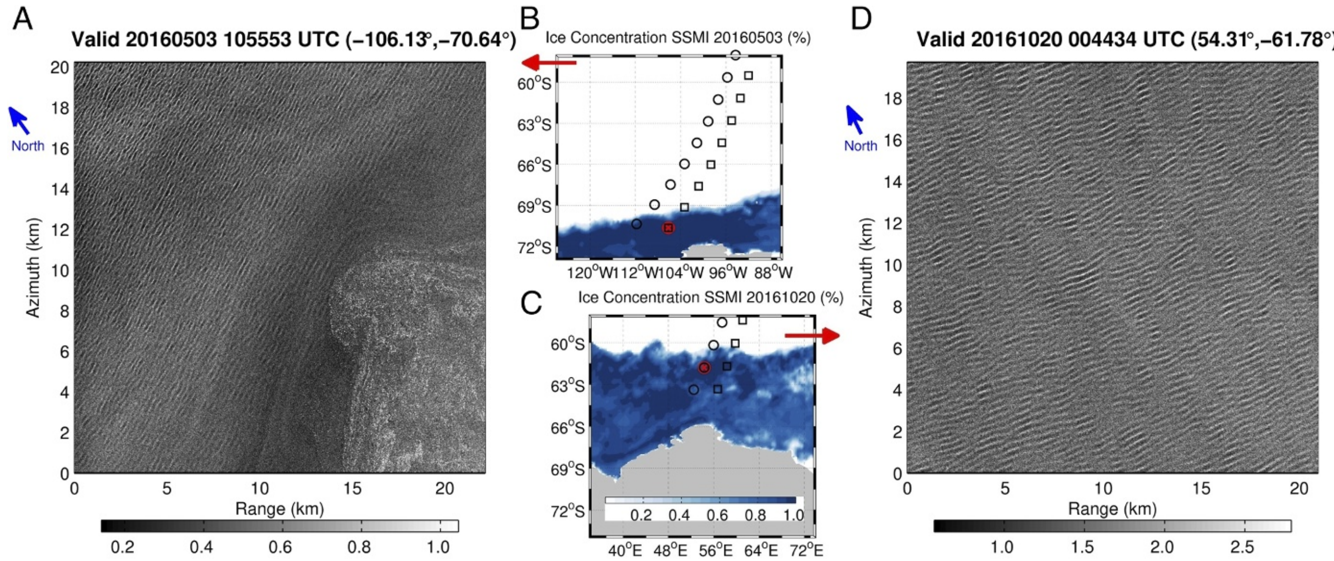

Fig. 1. S1A SAR sea surface roughness images acquired in the Amundsen Sea. (*A*) Rapid attenuation within a single image located 130 km into the ice. The top left corner of the image is closest to the ice edge with a wave height of 1.25 m ($E = 0.1$ m^2), wavelength of 230 m, and propagating from the northwest (330°). After several kilometers (range = 14, azimuth = 12 km), the wave height decreases to 0.4 m ($E = 0.01$ m^2) and the waves nearly vanish in the bottom right of the image, giving an exponential decay $\alpha = 3.4 \times 10^{-4}$ m^{-1}. (*B* and *C*) Daily sea-ice concentration from Special Sensor Microwave Imager (SSM/I) corresponding to S1A acquisition in *A* and *D*, respectively. (*D*) A uniform swell observed 150 km into the ice. The wave height is nearly constant at 0.5 m with a wavelength of 330 m propagating from the north (355°). The open ocean wave height is 4.2 m, which gives an exponential attenuation rate of $\alpha = 3.1 \times 10^{-5}$ m^{-1}.

ice-free scenes (24, 25). Using numerical model results over the open ocean gives similar results.

We also estimated the wind stress because it is known to be a dominant forcing mechanism in the region (8, 26) and it provides a useful scale to which the wave stress can be compared. A complete momentum balance would require knowledge of ice properties and internal stresses, which are not available. The wind stress is calculated using the Climate Forecast System Reanalysis (27, 28) near surface wind vectors at 10 m elevation (spatial resolution of 0.2°). We neglect the sea ice velocity compared with the wind speed and calculate the wind stress using the quadratic formulation and drag coefficients based on observations in the

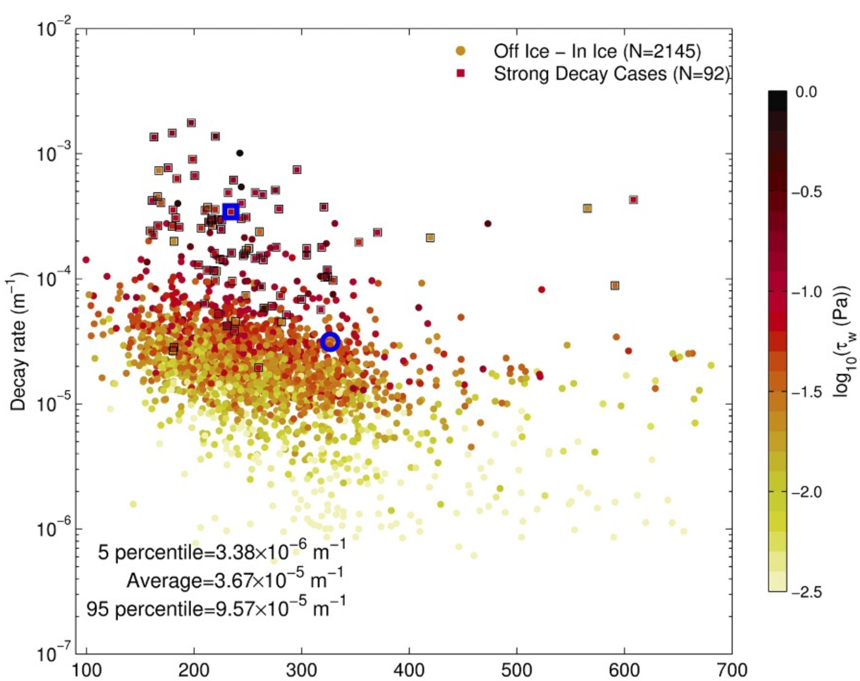

Fig. 2. Wave attenuation and stress: the relationship between the wavelength (abscissa), exponential wave energy decay rate (ordinate), and wave stress (color on logarithmic scale) is shown. Squares represent attenuation rates computed within one SAR image (92 cases), and circles represent attenuation rates computed using the gradient between the off-ice and in-ice observations (2,145 cases). The blue circle and square correspond to Fig. 1 *A* and *D*, respectively.

Weddell Sea (29–31) (see *Methods*). We computed the wind stress at the same time as the SAR observation to ensure consistent sampling.

Results

The distribution of the 2,237 estimates of wave decay rates $\alpha = -\log(E/E_0)/(x - x_0)$ is shown in Fig. 2, as a function of wavelength. In general, we observe stronger attenuation for shorter wavelengths, consistent with previous measurements and theories of wave–ice interactions (32). The more striking feature is the very large scatter, spanning 3 orders of magnitude, with a median around 3×10^{-5} m^{-1}.

Images with strong decay within the 20 km of the image ($\Delta H_s > 0.5$ m; e.g., Fig. 1*A*) are analyzed separately. We observe attenuation rates as high as $\alpha = 1.3 \times 10^{-3}$ m^{-1}, larger than previously observed for wavelengths larger than 100 m (16). The energy loss from the waves corresponds to a wave stress in their direction of propagation. The color scale in Fig. 2 highlights that wave stress increases with increasing wave attenuation, reaching values up to 1 Pa. Such high stresses combined with the

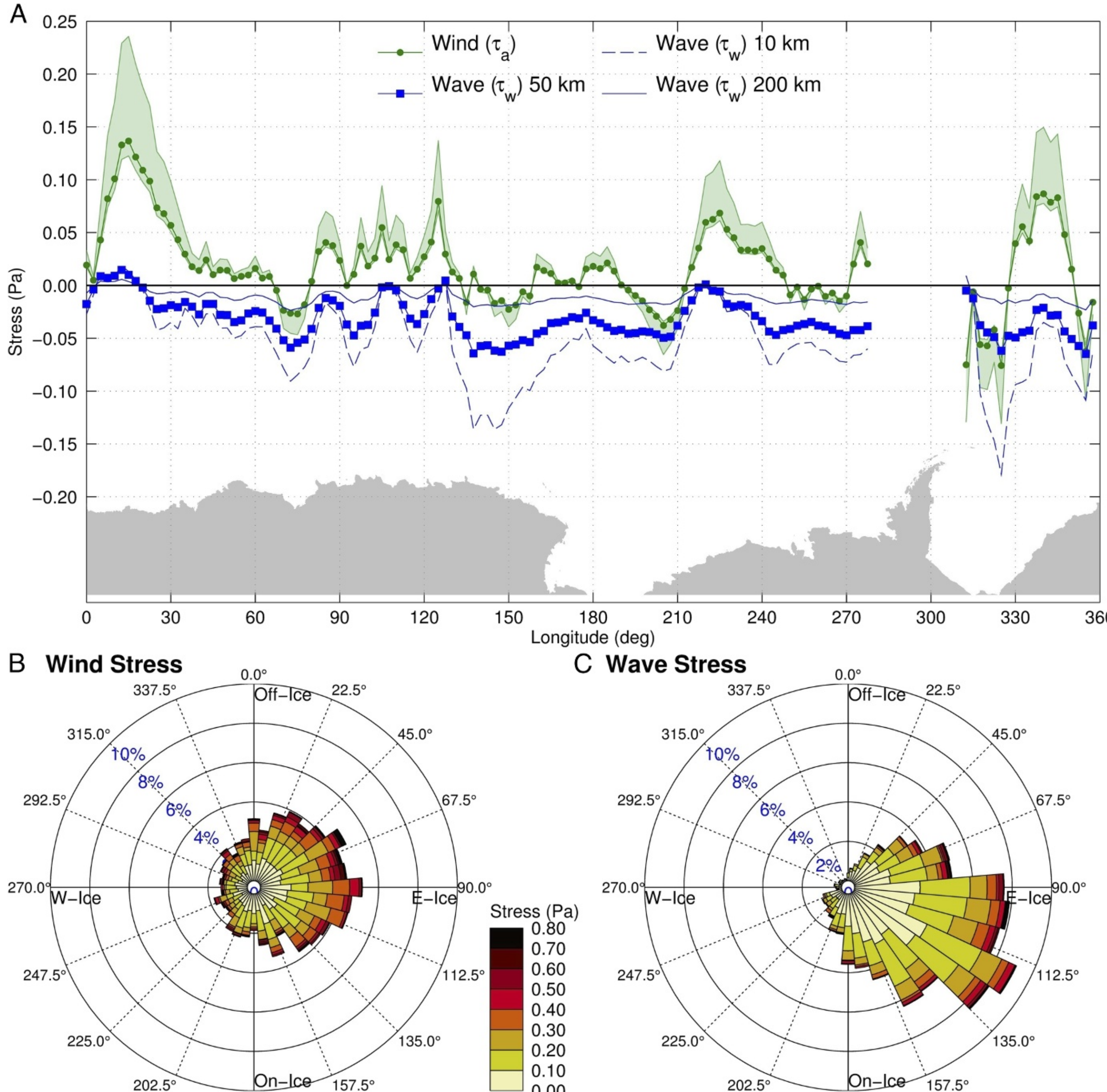

Fig. 3. Wind and wave stresses computed from the Climate Forecast System Reanalysis (CFSR) and S1 SARs (2014–2016). (*A*) The average wind (green) and wave (blue) stress per 5° longitude bin. The shading on the wind stress represents the expected variability based on the lower and upper bounds of the drag coefficients estimated in the Weddell Sea. The gray shading represents Antarctic for reference. *B* shows the CFSR wind stress, and *C* shows the wave stress at 10 km as a function of probability, magnitude, and direction (flowing-to) relative to the ice edge.

wave-induced orbital motion may lead to rafting (33). A positive feedback of rafted ice causing stronger wave dissipation due to friction between ice plates may lead to more rafting. In the absence of detailed measurements on the ice thickness and floe sizes, it is impossible to further evaluate this idea. However, the high wave stresses could be related to the observed thick and deformed ice reported in ref. 7, which appears in ridges with scales smaller than those found in the Arctic. Besides rafting, wave motion certainly contributes to the compaction of the ice edge. Compaction and rafting due to wave stresses may contribute to the larger roughness of sea ice, commonly observed by scatterometers in the outer belt of the Southern Ocean sea ice (26).

Here, we compare the average wind and wave stresses. Assuming the wave decay is exponential, we estimate the wave energy as a function of distance from the ice edge. In Fig. 3*A* we show the average wind and wave stresses as a function of longitude from 2014 to 2016. Due to the exponential decay, the stress over the first 10 km of ice is much higher than that across 50 km or 200 km. At nearly all longitudes, the wave stress is directed into the sea ice, with an average stress of -0.06 Pa over the first 10 km (we take the convention that stress in the off-ice direction is positive). A key feature of Fig. 3 is the opposing directions of mean wind and wave forcing. The wind stress is directionally variable (Fig. 3*B*) and results in an average of $+0.02$ Pa. This off-ice wind stress is consistent with other studies (8, 26). Conversely, the net wave stress (Fig. 3*C*) is generally directed into the sea ice (80%) and observed in both the freeze and melt seasons. These observations are consistent with the idea that, as storms traverse the area, the wind direction rapidly changes, while the waves are steadily directed into the ice. At larger scales, the observations suggest two important points:

- Over large areas of the marginal ice zone (MIZ), wave stress is of similar order to wind stress, meaning that wave forcing is significant for the overall dynamics of the MIZ.
- On-ice forcing by the wave field provides a stabilizing effect on the outer MIZ.

We expect that this consistent wave forcing reduces advective expansion of the Antarctic ice pack and reduces divergence of the MIZ.

Conclusion

The large scatter of decay rates shows that off-ice H_s alone does not determine the wave attenuation for the entire journey of a wave packet in sea ice. Our subset of 92 cases with strong local damping demonstrates that the waves can rapidly decrease (Fig. 2), and the same wave train can experience a weak attenuation over hundreds of kilometers and suddenly disappear over just a few kilometers. Using the wave decay relations provided in ref. 10 (or our estimates in *SI Appendix*) for the cases with the off-ice H_s would yield an attenuation rate that is much less than the rapid attenuation we observed and maximum wave stresses much weaker than the 1 Pa found here. These results show that wave attenuation is more dynamic and complex than reported in previous studies, and using a single attenuation rate for decay over variable sea-ice cover may not be sufficient.

Climate and seasonal ice models have difficulties in predicting sea-ice evolution, suggesting that important physical processes are not properly captured. Our observations derived from S1 SAR imagery show that wave stresses are important external forces on the sea ice within a few hundreds of kilometers of the ice edge and these stresses are highly variable. Clearly, the strong year-round wave forcing in the Southern Ocean (34) provides a significant force that should help maintain a compact ice edge. The associated wave motions likely also contribute to floe breakup and rafting, resulting in the rougher (and potentially thicker) sea ice observed by scatterometers near the ice edge (26). We expect that hotspots of wave decay and wave stress are caused by thicker ice, which itself may be favored by higher wave stresses.

In general, any SAR operated in high-resolution mode can provide wave measurements in sea ice. Using the extensive and systematic wave mode SAR data from the earlier ERS and Envisat missions, it should be possible to investigate waves around the sea ice with the same method, providing a climate record that is 25 y long and counting. These wave mode data also provide complementary information on winds over the open ocean (35, 36). The present dataset should be a useful testbed for the coupled wave–ice interaction models now under development. Such models may lead to improved predictability of sea-ice evolution, a key component of the Earth system.

Methods

We consider, without loss of generality, an ice edge along the y axis, with an x axis pointing into the ice, and a narrow wave spectrum propagating toward direction θ relative to the x axis. We use linear wave theory in deep water for wavelengths much longer than the ice thickness. The on-ice flux of momentum due to the wave motion in Nm^{-1} is

$$S_{xx} = \frac{1}{2} E \cos^2\theta, \qquad [1]$$

where E is the variance of the sea surface elevation and θ is the incident wave direction relative to the ice edge. The on-ice wave stress in Pa is the convergence of this flux, namely

$$\tau_w = -\frac{1}{2} \rho_w g \frac{\partial E}{\partial x} \cos^2 \theta, \qquad [2]$$

where ρ_w is the density of water and g is the gravity acceleration. Eq. **2** states that the wave stress is related to gradient in wave energy $\partial E/\partial x$. In the case of exponential decay $E \propto E_0 \exp(-\alpha x)$, this gradient is estimated from the ratio E/E_0 and the distance x between the two locations where E and E_0 are measured (10, 16).

Our SAR observations provide the in-ice significant wave height for each location j:

$$H_{s,j} = 4\sqrt{E_j}, \qquad [3]$$

with the surface elevation variance obtained from the 2D wave spectrum, $F(k_x, k_y)$, by

$$E_j = \int_{-0.8}^{0.8} \int_{-0.8}^{0.8} F(k_x, k_y) dk_x dk_y, \qquad [4]$$

where k_x and k_y are the wavenumbers in range and azimuth directions. The wave spectrum is obtained from the normalized radar backscatter image (21). Specific details on the SAR processing are provided in *SI Appendix*.

Neglecting the motion of the sea ice compared with the wind speed, we calculate the wind stress

$$\tau_a = \rho_a C_a U_a^2 \cos\theta, \qquad [5]$$

where ρ_a is the air density and θ represents the incident wind direction relative to the ice edge normal. Only a few studies estimate drag coefficients (C_a) in Antarctic sea ice; we use an average of 1.45×10^{-3} based on observations in the Weddell Sea (29–31) with a lower limit of 1.3×10^{-3} and upper limit of 2.5×10^{-3}. The wind speed (U_a) and direction relative to the ice edge (θ) are taken from the Climate Forecast System Reanalysis (CFSR) (28).

ACKNOWLEDGMENTS. We thank the European Commission and European Space Agency (ESA) for extending S1 wave mode acquisitions over sea ice. All authors are supported by Labex Mer via Grant ANR-10-LABX-19-01, the EU-FP7 project Ships and Waves Reaching Polar Regions (SWARP) under Grant Agreement 607476, Office of Naval Research (ONR) Grant N0001416WX01117, and the National Centre for Space Studies (CNES) project Wave–Ice.

1. Parkinson CL, Cavalieri DJ (2012) Antarctic sea ice variability and trends, 1979–2010. *Cryosphere* 6:871–880.
2. Gagne ME, Gillett NP, Fyfe JC (2015) Observed and simulated changes in Antarctic sea ice extent over the past 50 years. *Geophys Res Lett* 42:90–95.
3. Parkinson CL, DiGirolamo NE (2016) New visualizations highlight new information on the contrasting Arctic and Antarctic sea-ice trends since the late 1970s. *Remote Sens Environ* 183:198–204.
4. Turner J, Comiso J (2017) Solve Antarctica's sea-ice puzzle. *Nature* 547:275–277.

5. Marshall DP, Zanna L (2014) A conceptual model of ocean heat uptake under climate change. *J Clim* 27:8444–8465.
6. Turner J, Bracegirdle TJ, Phillips T, Marshall GJ, Hosking JS (2013) An initial assessment of Antarctic sea ice extent in the CMIP5 models. *J Clim* 26:1473–1484.
7. Williams G, et al. (2014) Thick and deformed Antarctic sea ice mapped with autonomous underwater vehicles. *Nat Geosci* 8:61–67.
8. Holland PR (2014) The seasonality of Antarctic sea ice trends. *Geophys Res Lett* 41:4230–4237.
9. Abernathey RP, et al. (2016) Water-mass transformation by sea ice in the upper branch of the southern ocean overturning. *Nat Geosci* 9:596–601.
10. Kohout AL, Williams MJM, Dean SM, Meylan MH (2014) Storm-induced sea-ice breakup and the implications for ice extent. *Nature* 509:604–607.
11. Collard F, Ardhuin F, Chapron B (2009) Monitoring and analysis of ocean swell fields from space: New methods for routine observations. *J Geophys Res* 114: C07023.
12. Longuet-Higgins MS (1977) The mean forces exerted by waves on floating or submerged bodies with applications to sand bars and wave power machines. *Proc R Soc A: Math Phys Eng Sci* 352:463–480.
13. Masson D (1991) Wave-induced drift force in the marginal ice zone. *J Phys Oceanogr* 21:3–10.
14. Liu AK, Häkkinen S, Peng CY (1993) Wave effects on ocean-ice interaction in the marginal ice zone. *J Geophys Res* 98:10025–10036.
15. Perrie W, Hu Y (1996) Air–ice–ocean momentum exchange. Part 1: Energy transfer between waves and ice floes. *J Phys Oceanogr* 26:1705–1720.
16. Wadhams P, Squire VA, Goodman DJ, Cowan AM, Moore SC (1988) The attenuation rates of ocean waves in the marginal ice zone. *J Geophys Res* 93:6799–6818.
17. Squire VA (1989) Super-critical reflection of ocean waves: A new factor in ice-edge dynamics? *Ann Glaciol* 12:157–161.
18. Wadhams P, Holt B (1991) Waves in frazil and pancake ice and their detection in seasat synthetic aperture radar imagery. *J Geophys Res* 96:8835–8852.
19. Schulz-Stellenfleth J, Lehner S (2002) Spaceborne synthetic aperture radar observations of ocean waves traveling into sea ice. *J Geophys Res* 107:C000837.
20. Ardhuin F, et al. (2015) Estimates of ocean wave heights and attenuation in sea ice using the SAR wave mode on Sentinel-1A. *Geophys Res Lett* 42:2317–2325.
21. Ardhuin F, et al. (2017) Measuring ocean waves in sea ice using SAR imagery: A quasi-deterministic approach evaluated with Sentinel-1 and in-situ data. *Remote Sens Environ* 189:211–222.
22. Stopa JE, et al. (2018) Wave attenuation through an Arctic Marginal Ice Zone on October 12, 2015. Part 1: Measurement of wave spectra and ice features from Sentinel-1A, 10.1029/2018JC013791
23. Ardhuin F, et al. (2018) Wave attenuation through an Arctic marginal ice zone on October 12, 2015. Part 2: Numerical modeling of waves and associated ice break-up. *J Geophys Res* 10.1002/2018JC013784.
24. Schulz-Stellenfleth J, König T, Lehner S (2007) An empirical approach for the retrieval of integral ocean wave parameters from synthetic aperture radar data. *J Geophys Res* 112:C03019.
25. Stopa JE, Mouche A (2017) Significant wave heights from Sentinel-1 SAR: Validation and applications. *J Geophys Res* 122:1827–1848.
26. Nghiem S, Rigor I, Clemente-Colon P, Neumann G, Li P (2016) Geophysical constraints on the Antarctic sea ice cover. *Remote Sens Environ* 181:281–292.
27. Saha S, et al. (2010) The NCEP climate forecast system reanalysis. *Bull Am Meteorol Soc* 91:1015–1057.
28. Saha S, et al. (2014) The NCEP climate forecast system version 2. *J Clim* 27:2185–2208.
29. Wamser C, Martinson DG (1993) Drag coefficients for winter Antarctic pack ice. *J Geophys Res* 98:12431–12437.
30. Andreas EL, Claffey KJ (1995) Air-ice drag coefficients in the western Weddell Sea: 1. Values deduced from profile measurements. *J Geophys Res* 100:4821–4831.
31. Fisher R, Lytle VI (1998) Atmospheric drag coefficients of Weddell Sea ice computed from roughness profiles. *Ann Glaciol* 27:455–460.
32. Squire VA, Dugan JP, Wadhams P, Rottier PJ, Liu AK (1995) Of ocean waves and sea ice. *Annu Rev Fluid Mech* 27:115–168.
33. Shen HH, Ackley SF, Hopkins MA (2001) A conceptual model for pancake-ice formation in a wave field. *Ann Glaciol* 33:361–367.
34. Hemer MA, Church JA, Hunter JR (2009) Variability and trends in the directional wave climate of the southern hemisphere. *Int J Climatol.* 30:475–491.
35. Lehner S, Schulz-Stellenfleth J, Schättler B, Breit H, Horstmann J (2000) Wind and wave measurements using complex ERS-2 SAR wave mode data. *IEEE Trans Geosci Remote Sens* 38:2246–2257.
36. Horstmann J, Schiller H, Schulz-Stellenfleth J, Lehner S (2004) Global wind speed retrieval from SAR. *IEEE Trans Geosci Remote Sens* 41:2277–2286.